Suppression of servo error uncertainty to 10^{-18} level using double integrator algorithm in ion optical clock

Jin-Bo Yuan(袁金波), Jian Cao(曹健), Kai-Feng Cui(崔凯枫), Dao-Xin Liu(刘道信), Yi Yuan(袁易), Si-Jia Chao(晁思嘉), Hua-Lin Shu(舒华林), and Xue-Ren Huang(黄学人)

Citation: Chin. Phys. B, 2021, 30 (**7**): 070305. DOI: 10.1088/1674-1056/abf918
Journal homepage: http://cpb.iphy.ac.cn; http://iopscience.iop.org/cpb

What follows is a list of articles you may be interested in

Efficient self-testing system for quantum computations based on permutations

Shuquan Ma(马树泉), Changhua Zhu(朱畅华), Min Nie(聂敏), and Dongxiao Quan(权东晓)
Chin. Phys. B, 2021, 30 (**4**): 040305. DOI: 10.1088/1674-1056/abe29a

A proposal for preparation of cluster states with linear optics

Le Ju(鞠乐), Ming Yang(杨名), and Peng Xue(薛鹏)
Chin. Phys. B, 2021, 30 (**3**): 030306. DOI: 10.1088/1674-1056/abd74b

Quantum algorithm for a set of quantum 2SAT problems

Yanglin Hu(胡杨林), Zhelun Zhang(张哲伦), and Biao Wu(吴飙)
Chin. Phys. B, 2021, 30 (**2**): 020308. DOI: 10.1088/1674-1056/abd741

Review of quantum simulation based on Rydberg many-body system

Zheng-Yuan Zhang(张正源), Dong-Sheng Ding(丁冬生), and Bao-Sen Shi(史保森)
Chin. Phys. B, 2021, 30 (**2**): 020307. DOI: 10.1088/1674-1056/abd744

Selected topics of quantum computing for nuclear physics

Dan-Bo Zhang(张旦波), Hongxi Xing(邢宏喜), Hui Yan(颜辉), Enke Wang(王恩科), and Shi-Liang Zhu(朱诗亮)
Chin. Phys. B, 2021, 30 (**2**): 020306. DOI: 10.1088/1674-1056/abd761

Suppression of servo error uncertainty to 10^{-18} level using double integrator algorithm in ion optical clock*

Jin-Bo Yuan(袁金波)[1,2,3], Jian Cao(曹健)[1,2,†], Kai-Feng Cui(崔凯枫)[1,2], Dao-Xin Liu(刘道信)[1,2,3], Yi Yuan(袁易)[1,2,3], Si-Jia Chao(晁思嘉)[1,2], Hua-Lin Shu(舒华林)[1,2], and Xue-Ren Huang(黄学人)[1,2,‡]

[1] *State Key Laboratory of Magnetic Resonance and Atomic and Molecular Physics, Innovation Academy for Precision Measurement Science and Technology, Chinese Academy of Sciences, Wuhan* 430071, *China*

[2] *Key Laboratory of Atomic Frequency Standards, Innovation Academy for Precision Measurement Science and Technology, Chinese Academy of Sciences, Wuhan* 430071, *China*

[3] *University of Chinese Academy of Sciences, Beijing* 100049, *China*

(Received 10 March 2021; revised manuscript received 31 March 2021; accepted manuscript online 19 April 2021)

A universal locking model for single ion optical clocks was built based on a simple integrator and a double integrator. Different integrator algorithm parameters have been analyzed in both numerical simulations and experiments. The frequency variation measured by the comparison of two optical clocks coincides well with the simulation results for different second integrator parameters. According to the experimental results, the sensitivity of the servo error influenced by laser frequency drift with the addition of a double integrator was suppressed by a factor of 107. In a week-long comparison of optical clocks, the relative uncertainty of the servo error is determined to be 1.9×10^{-18}, which is meaningful for the systematic uncertainty of the transportable single $^{40}Ca^{+}$ ion optical clock entering the 10^{-18} level.

Keywords: optical clocks, frequency uncertainty, servo error, servo algorithm

PACS: 03.67.Ac, 03.67.Pp, 06.30.Ft **DOI:** 10.1088/1674-1056/abf918

1. Introduction

Owing to the developments in ultracold atomic systems and the improvement in laser frequency stabilization technology, optical clocks have achieved a better performance over the past few decades. As a competitive candidate for the next-generation second definition,[1] the frequency stability and uncertainty of optical clocks have been rapidly developing.[2–8] Meanwhile, in different application areas, such as chronometric leveling, the measurement of the fundamental constants, and the search for dark matter, higher demands for a higher frequency stability and uncertainty have been raised.[9–12]

As a connector, the servo algorithm adjusts the frequency of optical local oscillator into resonance with the clock transition, realizing automatic interrogation and locking of the clocks. In a simple integrator algorithm, the servo error caused by laser frequency drift may become an obstacle in uncertainty evaluation of high-precision optical clocks. Adding a second integrator after the simple integrator is effective in suppressing the servo error caused by linear frequency drift.[13–16] However, in these studies, servo error evolution functions evolving with different second integrator parameters are not mentioned, and only empirical parameters are given. To accurately determine the second integrator parameters when applied to an optical clock under different circumstances, it is necessary to evaluate how the servo error varies with the variation of the second integrator parameters.

In this paper, we built an optical clock locking model to investigate the servo error variation with different second integrator parameters. According to the simulations, the sensitivity of the servo error influenced by laser frequency drift is suppressed as a function of experimental decay when second integrator parameters increase. To demonstrate the simulation results, we measured the frequency variation of the clock with different second integrator parameters. The frequency variation coincides well with the simulation results for different second parameters. A rejection ratio of 107 was achieved when the double integrator algorithm was employed. The servo error uncertainty of the clock was evaluated as 1.9×10^{-18}, operating with optimal double integrator parameters for a week while all other parameters remain the same, improved by an order of magnitude.

2. Numerical simulation

For single ion optical clocks, interrogation must be repeated dozens of times to obtain quantum jumps and calculate the excitation probability when the servo algorithm is applied. The electron shelving scheme[17,18] is used for the quantum jump experiments in our single $^{40}Ca^{+}$ ion optical clock. The four-point locking scheme[19,20] is used to maintain the detection laser resonance with the clock transition. Suppose that the interrogation laser frequency of the n-th servo interval is f_n, closed to the center of the resonance line, and that the

*Project supported by the National Key Research and Development Program of China (Grant No. 2017YFA0304404) and the National Natural Science Foundation of China (Grant No. 11674357).

†Corresponding author. E-mail: caojian@apm.ac.cn

‡Corresponding author. E-mail: hxueren@apm.ac.cn

full width at half maximum (FWHM) of the resonance spectrum is 2δ. The detection laser frequency can be expressed as $f_{\rm l} = f_n - \delta$ and $f_{\rm r} = f_n + \delta$. The error signal e_n of the n-th servo interval can be calculated as follows:

$$e_n = \delta \cdot \frac{N_{\rm l} - N_{\rm r}}{N_{\rm l} + N_{\rm r}}. \tag{1}$$

Laser frequency of the next interval is

$$f_{n+1} = f_n - G \cdot e_n, \tag{2}$$

where G is the gain of the simple servo algorithm, $G \cdot e_n$ is the n-th frequency correction applied before the $n+1$ interval is started, and $N_{\rm l}$ and $N_{\rm r}$ are the quantum jump numbers, respectively.

Because the simple servo algorithm only includes information of the laser frequency and error signal during the n-th servo interval, it will cause a servo error if the laser frequency drifts during the $n+1$ servo interval. A correction based on laser frequency drift prediction should be added to the algorithm to reduce the servo error, which is the so-called second integrator. For a perfect servo algorithm, the sum of the error signal should be zero over a long period of time. It significantly deviates from zero when a servo error exists, which means that the sum of the error signal can be considered as an indicator of servo error caused by laser frequency drift. The recurrence formula of the double-integrator servo algorithm becomes

$$f_{n+1} = f_{n+1} - G \cdot e_n - I \cdot \sum_{i=n-m+1}^{m} e_i, \tag{3}$$

where the second integrator gain I is added as a factor to adjust the servo response to laser frequency drift, and m is the number of errors counted to calculate the sum of the error signal, corresponding to the second integration time.

2.1. Simulation of the simple integrator algorithm

We built a single ion optical locking model with parameters based on the clock-locking process to simulate the servo error variation by different algorithms. The linewidth of the clock transition is 13.4 Hz, corresponding to a probe time of 60 ms. The linear drift of laser frequency changes within the range of −25 mHz/s to +25 mHz/s, and each servo interval takes 10 s to complete the interrogation of the spectrum, leading to a frequency change between −250 mHz and +250 mHz after one servo finishing.

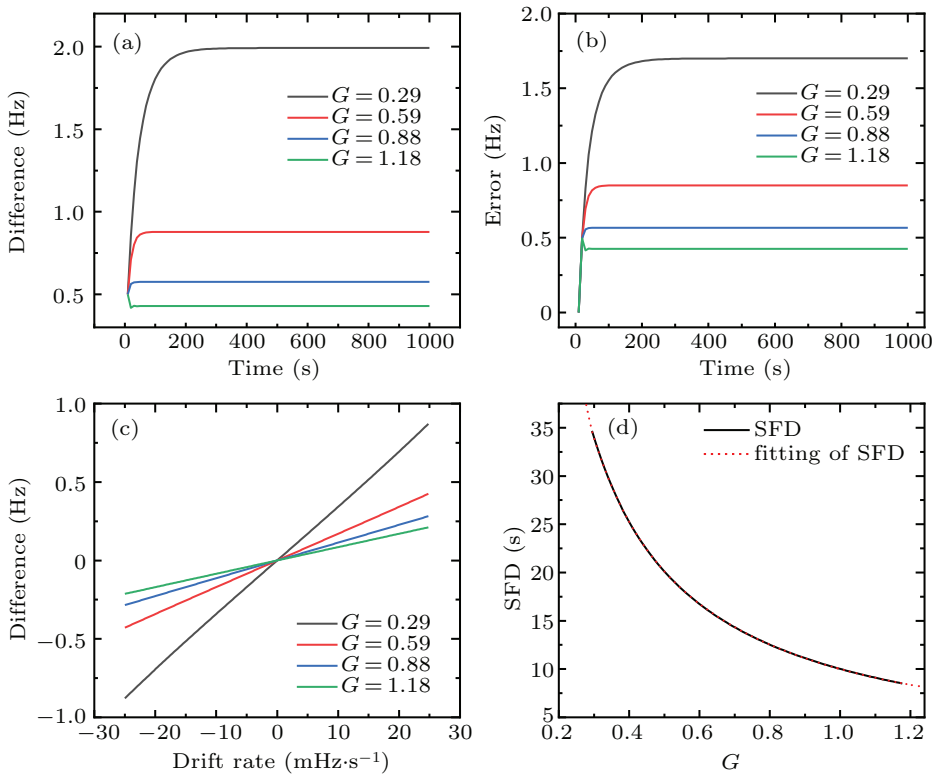

Fig. 1. Simulations of servo response and servo error evaluation at a 50-mHz/s laser drift rate under a simple integrator algorithm. The curves are labeled by simple integrator gain G: (a) variation of frequency difference over time since algorithm started, (b) variation of servo error over time since algorithm started, (c) variation of frequency difference over frequency linear drift rate, and (d) variation of SFD over gain G of simple integrator. Red dashed curve shows the experimental decay fitting of SFD.

The simple integrator algorithm was the first to be investigated in our locking model. The servo error and frequency response under different gains G are depicted in Fig. 1 with different colored curves. When the laser frequency increases at a rate of 50 mHz/s, the frequency difference changes since locking starts, as shown in Fig. 1(a). As the simple integrator gain G increases, the time required for the servo to stabilize becomes shorter and the stable state difference decreases

at the same time. The error signal shares a similar rule with the frequency difference over time, as shown in Fig. 1(b). In the following discussion of this paper, we consider the frequency difference as the main research object. In Fig. 1(c), the frequency difference between the detection laser and clock transition varies linearly with drift rate when the gains are optimized. The slope of the lines in Fig. 1(c) represents the sensitivity of the servo error influenced by the linear frequency drift, which is abbreviated as the slope of the frequency difference (SFD) in the following discussion. As shown in Fig. 1(d), the SFD decreases with simple integrator gain G according to the law of experimental decay. However, it is disappointing that a perfect servo algorithm cannot be realized, although the SFD becomes smaller while the simple integrator gains G increases. By contrast, the increment of the simple integrator gain G is ineffective after SFD reaches the saturation region. However, the over-feedback error signal derived from excessive gain may decrease the frequency stability of the optical clock.[21] Under a comprehensive consideration, the optimized simple integrator gain is set as $G = 1.0$. Based on a simple integrator algorithm with optimum gain, the residual servo error can be further suppressed by the addition of the second integrator.

2.2. Simulation of the double integrator algorithm

Similar to the simple integrator algorithm, we analyze the servo response of the double integrator algorithm from the aspects of time, drift rate, and SFD. The simple integrator gain is set as $G = 1.0$, throughout the double integrator algorithm simulation process. In Figs. 2(a) and 2(b), the second integrator gain I and quantum projection noise were considered simultaneously under the second integrator number $m = 50$. Benefitting from the increase in the second integrator gain I, the frequency difference caused by laser frequency drift decreases dramatically and oscillates for a longer time, reaching the limit when I approaches 1/10 of G in Fig. 2(a). The oscillation will not constrict if the second integrator gain I is too large.

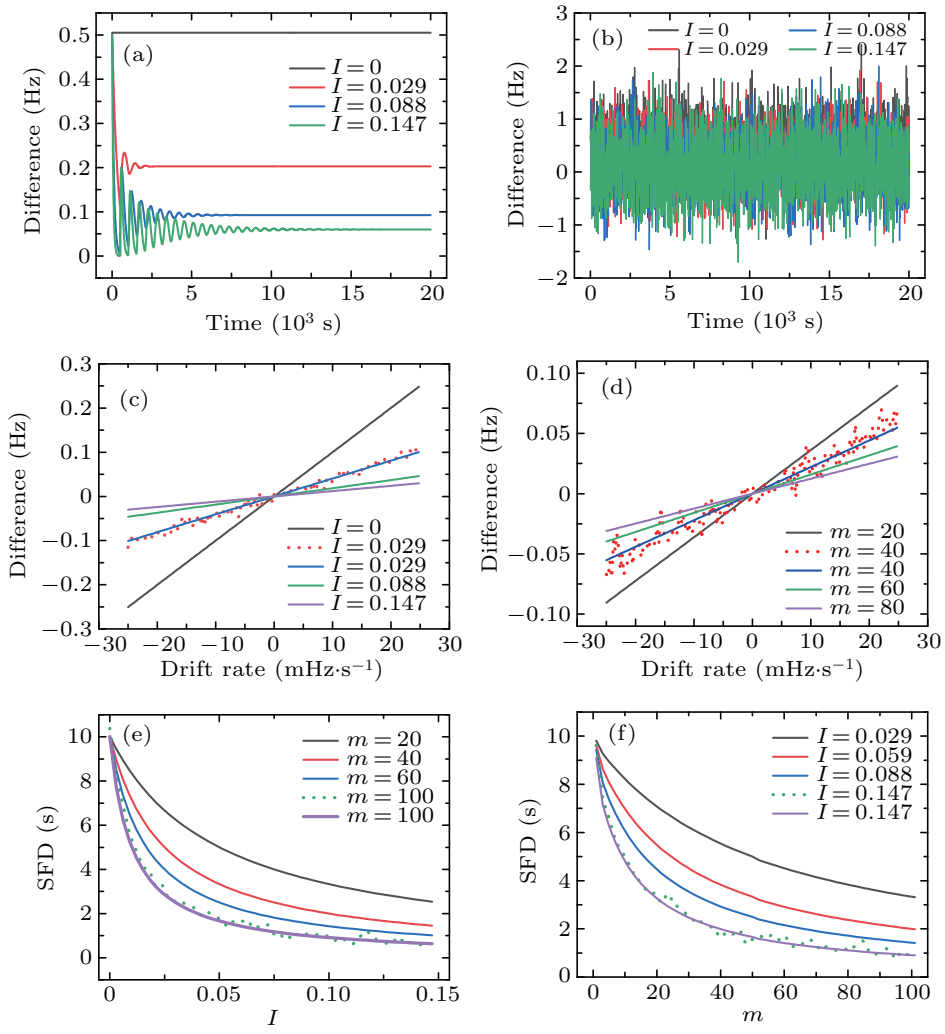

Fig. 2. Simulations of servo response evaluation under double integrator algorithm. The simple integrator gain is set as $G = 1.0$ throughout the simulation process. Simulation with QPN is labeled by the red dashed line in panels (c)–(f). Variations of servo response to a 50-mHz/s drift rate (a) without QPN after the algorithm starts and (b) with QPN. Curves in both graphs are labeled by second integrator gain I. Variation of frequency difference over frequency linear drift rate labeled by (c) second integrator gain I when $m = 50$ and (d) second integrator number m when $I = 0.088$. (e) Variation of SFD over gain I of second integrator when $m = 50$. (f) Variation of SFD over m of the second integrator when $I = 0.088$.

The QPN is 8- to 20-times the servo error under the double integrator algorithm according to the amplitude of the frequency difference in panels (a) and (b). To minimize the effect of QPN, the frequency differences of detection laser and clock transition are averaged for 2×10^4 s after the oscillation becomes stabilized when analyzing the SFD. The same strategy is implemented for the frequency difference evaluation in clock comparison experiments.

Both the second integrator parameters I and m have an impact on the frequency difference, as shown in Figs. 2(c) and 2(d). The curves in Figs. 2(e) and 2(f) illustrate the variation of the SFD over the second integrator parameters I and m, respectively. In Figs. 2(c)–2(f), simulations without QPN are labeled as solid lines and those with QPN are indicated by dashed lines. The SFD is suppressed as a function of experimental decay when second integrator parameters I or m increases. Both the second integrator parameters I and m are indispensable, and the improper setting of either will make the servo error more sensitive to laser frequency drift. It is also demonstrated that QPN will not have an effect on the servo when averages are taken, according to the dashed curves shown in Figs. 2(c)–2(f), where the variation is randomly distributed around curves without QPN.

3. Experimental set up

The double integrator algorithm was applied to both $^{40}Ca^{+}$ transportable clocks involved in the frequency comparison with all other parameters being constant. The aspects of clock 1 are the same as those mentioned in our previous study,[22] except that the ring trap is replaced by a linear Paul trap. Clock 2 is a newly established transportable optical clock that is more miniaturized and integrated than clock 1. All lasers and optical components involved in clock 2 are integrated into a 75 cm $\times$35 cm$\times$25 cm module, and lasers are stabilized using a multi-channel cavity during clock operation.[23] In both clocks, measurements of three pairs of Zeeman components were taken to eliminate the electric quadrupole shift[24] while locking the clocks. As shown in Fig. 3, we measured three pairs of Zeeman components by changing the frequency shift of AOM 1 before trap 1. Frequency corrections are added to the frequency of AOM 1 during clock 1 locking, and the average frequency of three pairs of Zeeman components is applied to AOM 1′ when each servo interval is finished. The laser beam shifted by AOM 1′ was used for clock transition frequency output and clock comparison. Clock 2 shares the same locking scheme as clock 1. Throughout the comparison experiment, the two clock lasers are stabilized to two independent ultra-stable Fabry–Perot cavities using the Pound–Drever–Hall (PDH) technique.[23,25,26] The drift rate of the clock laser is controlled by adjusting the frequency sweeping speed of the AOM 1″ and AOM 2″ drivers before the cavity every 30 min.

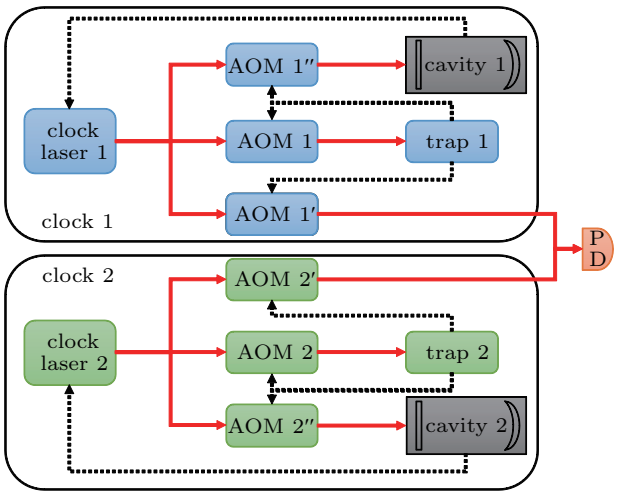

Fig. 3. Schematic diagram of comparison between two clocks. The optical path is denoted by red solid lines. The servo path is denoted by black dashed lines. AOM: acoustic optical modulator; PD: photodetector.

For one clock, the frequency change of the clock transition frequency output needs to be measured when evaluating optimum second integrator parameters. During the frequency comparison, clock 1 works as a reference clock, the laser frequency drift rate of which is compensated between -5 mHz/s and $+5$ mHz/s. The other works as an undetermined clock, the laser frequency drift rate of which varies from -80 mHz/s to $+80$ mHz/s. Because the laser frequency drift rate in clock 1 is much smaller than that in clock 2, the clock transition frequency output of clock 1 is much more stable than that of clock 2 even in simple integrator algorithm, according to the simulation. Thus, the clock transition frequency output of clock 2 mainly contributes to the frequency difference between the two clocks.

4. Experimental results

Figure 4 shows a typical process for determining the optimal second integrator parameters based on a series of frequency comparison between two clocks. First, we assess the influence of the second integrator gain I on the frequency difference between clock 1 and clock 2. As shown in Fig. 4(a), the frequency difference changes linearly with the drift rate of clock laser 2. Similar to the numerical simulation, we use the SFD as a key indicator in the servo parameter evaluation. When the second integrator number m is 30, five SFDs under different second integrator gains I are obtained and marked as black dots in Fig. 4(c). As can be seen from the figure, the SFD reduction becomes negligible when the second integrator gain I increases by more than 0.088. Second, the same approach was used to study the influence of the second integrator number m on the frequency difference, as shown in Fig. 4(b). In Fig. 4(d), the SFD under different second integrator numbers m displays a similar law as that in Fig. 4(c), except for a much smaller SFD value.

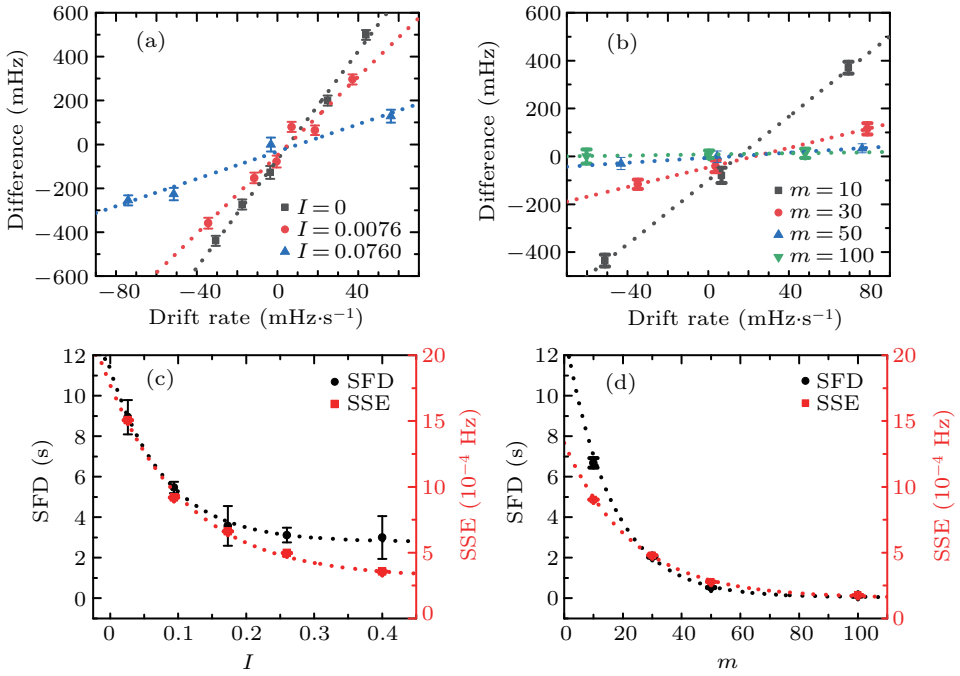

Fig. 4. Experimental results of frequency comparison between two clocks when determining optimal second integrator parameters. The laser frequency drift rate of clock laser 1 is compensated between −5 mHz/s and +5 mHz/s. (a) and (b) Frequency difference measured when the drift rate of clock laser 2 changes and linear fittings of the data are shown in dashed lines. Measurements in panel (a) are labeled with different second integrator gain I when $m = 30$ and that in panel (b) are labeled with a different second integrator number m when $I = 0.088$. (c) SFD and SSE under different second integrator gain I when $m = 30$. (d) SFD and SSE under different second integrator m when gain $I = 0.088$. The curve in black and red dashed line represents the experimental decay fitting of the SFDs and SSEs.

Finally, the slope of the servo error (SSE) to the drift rate has the same trend as the SFD throughout the comparison. Benefitting from the preferable second integrator parameters, the convergence of the SSE shown in Fig. 4(d) is smaller than that in Fig. 4(c). It is worth noting that SSE decreases more slowly than SFD when either the second integrator parameter I or m is small, which should be considered when the SSE is taken as an indicator for parameter optimization. Overall, the experimental results over the entire comparison process were in good agreement with the simulations. A rejection ratio of 107 was achieved by dividing the slope of the black dashed line in Fig. 4(a), and the green dashed line in Fig. 4(b). During a week-long locking of clock with optimized second integrator parameters and the remaining same parameters, the relative servo error uncertainty was determined to be 1.9×10^{-18}, which was enhanced by an order of magnitude compared to that only with the simple integrator algorithm.

5. Conclusion

In summary, we simulated the servo response and servo error of a single ion optical clock with different second integrator parameters. Frequency comparisons between two clocks were carried out to verify the simulation results. The experimental results coincided well with the simulation. With the optimized parameters, the SFD was suppressed by a factor of 107. The relative uncertainty of the servo error was evaluated as 1.9×10^{-18} during a week-long comparison of the clocks, a 10-fold improvement compared with the simple integrator algorithm under the same laser frequency drift rate. The double integrator algorithm has shown significant potential in building a 10^{-18} level optical clock.

Acknowledgment

The authors would like to thank Shaomao Wang and Ping Zhang for the preliminary work on the development of the transportable single $^{40}Ca^{+}$ ion optical clocks.

References

[1] Riehle F, Gill P, Arias F and Robertsson L 2018 *Metrologia* **55** 188
[2] Oelker E, Hutson R B, Kennedy C J, Sonderhouse L, Bothwell T, Goban A, Kedar D, Sanner C, Robinson J M, Marti G E, *et al.* 2017 *Nat. Photon.* **13** 714
[3] Brewer S M, Chen J S, Hankin A M, Clements E R, Chou C W, Wineland D J, Hume D B and Leibrandt D R 2019 *Phys. Rev. Lett.* **123** 033201
[4] Huntemann N, Sanner C, Lipphardt B, Tamm Chr and Peik E 2016 *Phys. Rev. Lett.* **116** 063001
[5] McGrew W F, Zhang X, Fasano R J, Schäffer S A, Beloy K, Nicolodi D, Brown R C, Hinkley N, Milani G, Schioppo M, *et al.* 2018 *Nature* **564** 87
[6] Lin Y G, Wang Q, Li Y, Meng F, Lin B K, Zang E J, Sun Z, Fang F, Li T C and Fang Z J 2015 *Chin. Phys. Lett.* **32** 090601
[7] Kong D H, Wang Z H, Guo F, Zhang Q, Lu X T, Wang Y B and Chang H 2020 *Chin. Phys. B* **29** 070602
[8] Sun Y X. Yao Y, Hao Y Q, Yu H F, Jiang Y Y and Ma L S 2020 *Chin. Phys. Lett.* **18** 070201
[9] Mehlstäubler T E, Grosche G, Lisdat C, Schmidt P O and Denker H 2018 *Rep. Prog. Phys.* **81** 064401
[10] Derevianko A and Pospelov M 2018 *Nat. Phys.* **10** 933
[11] Arvanitaki A, Huang J and Van T K 2015 *Phys. Rev. D* **91** 015015
[12] Safronova M S, Budker D, DeMille D, Kimball D F J, Derevianko A and Clark C W 2018 *Rev. Mod. Phys.* **90** 025008

[13] Bernard J E, Marmet L and Madej A A 1998 *Opt. Commun.* **150** 170
[14] Berkeland D J, Miller J D, Bergquist J C, Itano W M and Wineland D J 1998 *Phys. Rev. Lett.* **80** 2089
[15] Leroux I D, Scharnhorst N, Hannig S, Kramer J, Pelzer L, Stepanova M and Schmidt P O 2017 *Metrologia* **54** 307
[16] Zhang B L, Huang y, Zhang H Q, Hao Y M, Zeng M Y, Guan H and Gao K L 2020 *Chin. Phys. B* **29** 074209
[17] Sauter T h, Neuhauser W, Blatt R and Toschek P E 1986 *Phys. Rev. Lett.* **57** 1696
[18] Bergquist J C, Hulet R G, Itano W M and Wineland D J 1986 *Phys. Rev. Lett.* **57** 1699
[19] Barwood G, Gao K, Gill P, Huang G L and Klein H A 2001 *IEEE Trans. Instrum. Meas.* **50** 543
[20] Bernard J E, Madej A A, Marmet L, Whitford B G, Siemsen K J and Cundy S 1999 *Phys. Rev. Lett.* **82** 3228
[21] Peik E, Schneider T and Tamm C 2005 *J. Phys. B: At., Mol. Opt. Phys.* **39** 145
[22] Cao J, Zhang P, Shang J J, Cui K F, Yuan J B, Chao S J, Wang S M, Shu H L and Huang X R 2017 *Appl. Phys. B: Lasers Opt.* **123** 1
[23] Wang S M, Cao J, Yuan J B, Liu D X, Shu H L and Huang X R 2020 *Opt. Express* **28** 11852
[24] Margolis H S, Barwood G P, Huang G, Klein H A, Lea S N, Szymaniec K and Gill P 2004 *Science* **306** 1355
[25] Black E D 2001 *Am. J. Phys.* **69** 79
[26] Shang J J, Cao J, Cui K F, Wang S M, Zhang P, Yuan J B, Chao S J, Shu H L and Huang X R 2017 *Opt. Commun.* **382** 410